

# Explainable Deep Convolutional Multi-Type Anomaly Detection

Alex George<sup>[0009-0008-5799-4161]</sup>, Lyudmila Mihaylova<sup>[0000-0001-5856-2223]</sup>, and Sean Anderson<sup>[0000-0002-7452-5681]</sup>

School of Electrical and Electronic Engineering, University of Sheffield, UK  
`{ageorge4,l.s.mihaylova,s.anderson}@sheffield.ac.uk`

**Abstract.** Most explainable anomaly detection methods often identify anomalies but lack the capability to differentiate the type of anomaly. Furthermore, they often require the costly training and maintenance of separate models for each object category. The lack of specificity is a significant research gap, as identifying the type of anomaly (e.g., “Crack” vs. “Scratch”) is crucial for accurate diagnosis that facilitates cost-saving operational decisions across diverse application domains. While some recent large-scale Vision-Language Models (VLMs) have begun to address this, they are computationally intensive and memory-heavy, restricting their use in real-time or embedded systems. We propose MultiTypeFCDD, a simple and lightweight convolutional framework designed as a practical alternative for explainable multi-type anomaly detection. MultiType-FCDD uses only image-level labels to learn and produce multi-channel heatmaps, where each channel is trained to correspond to a specific anomaly type. The model functions as a single, unified framework capable of differentiating anomaly types across multiple object categories, eliminating the need to train and manage separate models for each object category. We evaluated our proposed method on the Real-IAD dataset and it delivers results competitive with state-of-the-art complex models at significantly reduced parametric load and inference times. This makes it a highly practical and viable solution for real-world applications where computational resources are tightly constrained.

**Keywords:** Deep Learning · Explainability · Multi-Type Anomaly Detection.

## 1 Introduction

Anomaly detection is a critical aspect in computer vision where the core objective is to identify patterns in visual data that do not conform to expected normal behaviour [27]. Recent years have witnessed significant adoption of deep learning-based anomaly detection in domains ranging from medical imaging [10], autonomous driving [5] to industrial manufacturing [1]. An important aspect of these sophisticated models is their explainability. Being able to understand why the model flagged something as an anomaly not only builds trust, but also helps the end users to make better and informed decisions, especially in sensitive areas

like healthcare and autonomous driving [2, 21]. By definition, anomalies are rare events, leading to a class imbalance where the normal samples vastly outnumber the abnormal ones [30]. Consequently, many state-of-the-art methods approach this problem of explainable anomaly detection from a one-class classification perspective [7, 8, 23, 24, 29].

A key limitation of all these methods is that they do not distinguish between different types of anomaly (unless separate models are trained for this purpose). This inhibits real-world decision making where understanding the type of anomaly is critical for determining the appropriate course of follow-up action [11]. For instance, in manufacturing metal parts, a system that can distinguish between a harmless discolouration and any rust or corrosion can trigger a simple cleaning process for the former, while initiating a more intensive grinding process or even scrapping the part entirely for the latter [3]. This characterisation is what enables an intelligent, cost-saving decision. Despite this clear need, the field of multi-type anomaly detection remains relatively unexplored [26].

Recently, methods have begun to address this problem by exploiting vision-language models (VLMs) [26, 32] combining text prompts with visual features to segment multiple defect types. However, these models are computationally intensive, leading to substantial energy consumption and these translate into significant carbon emissions and financial costs [28]. Additionally, such architectures are often not well suited to systems with tight constraints on computational power and latency [25], such as embedded systems, robotics and industrial automation. This highlights a clear need to explore alternative approaches that prioritise computational efficiency and practical deployability for real-world systems.

To address this research gap, our work proposes a novel deep convolutional multi-type anomaly detection method. We base the architecture on the Fully Convolutional Data Description (FCDD) [24] framework, extending it to produce multi-channel outputs, each corresponding to a distinct defect category, which we refer to as MultiTypeFCDD. We also develop a novel loss function to handle multiple types of anomaly. This enables the simultaneous detection and spatial localisation within an image for multiple pre-defined anomaly types. Our research addresses the general question: *Given a pre-defined set of anomaly types found in various objects, can we uniquely identify these anomalies in any given object using a lightweight and efficient model?* We demonstrate, on the publicly available Real-IAD dataset [38], that our proposed lightweight framework retains competitive performance to state of the art models while operating with significantly fewer parameters and lower inference times, making it a viable and practical solution for real-world applications with tight resource constraints.

## 2 Related Works

### 2.1 Deep Learning for Anomaly Detection

Early approaches for anomaly detection utilised classical machine learning methods such as One-Class Support Vector Machines (OC-SVM) [33], Support Vec-

tor Data Descriptions (SVDD) [37] and Isolation Forests [22]. Methods such as SVDD have been extended with deep learning methods in Deep SVDD [31] to improve the processing of complex data sets, which has improved performance in cases where it is challenging to obtain a useful feature representation [27].

## 2.2 Explainable Anomaly Detection and Segmentation

The black-box nature of deep learning models has driven the need to develop methods to aid transparency in the decision-making process [2]. Recent research have witnessed methods specifically designed for explainable anomaly detection, including feature-embedding methods such as PaDiM [7], PatchCore [29] and SoftPatch [20], and end-to-end trainable methods such as FCDD [24], SimpleNet [23] and Reverse Distillation (RD) [8].

As the above approaches rely on image-level labels (or no labels) rather than pixel-level annotations for training, they can be regarded as closely related to weakly supervised semantic segmentation (WSSS) [18, 39]. In WSSS, models produce dense pixel-wise maps from weak annotations such as image-level labels or bounding boxes. Consequently, anomaly detection and segmentation under weak supervision naturally aligns within this paradigm.

## 2.3 Multi-Class vs Multi-Type Anomaly Detection

The methods discussed above frame anomaly detection from a one-class classification perspective where the goal is to separate out a single type of anomaly from normal data. This approach is sufficient for many anomaly detection benchmarks such as MVTec-AD [4] and VisA [42].

Recent literature has started to explore and use the terminology “multi-class anomaly detection” [16, 19, 40], which typically refers to identifying single types of anomaly across multiple objects. Additionally, most existing models are designed to segment anomalies within a single object, meaning that separate models might be required to process each object.

Efforts have been made to create unified models for multi-class anomaly detection, such as UniAD [40]. However, these models cannot distinguish between different types of anomaly. In short, multi-type anomaly detection remains an area that is still under-explored [26].

## 2.4 Vision-Language Models for Anomaly Characterisation

Recent research has made use of vision-language models (VLMs) [6, 14, 17] to tackle multi-type anomaly detection. These models combine text prompts with image features, allowing them to both classify anomalies as well as create pixel-wise anomaly maps highlighting anomalous regions in the image. Two methods in particular, MultiADS [32] and VELM [26], have demonstrated this approach for industrial anomaly detection.

Despite their advantages, VLMs are generally heavy, computationally intensive and have higher inference time, making them less well suited to real-time or embedded systems [12, 28, 35].

## 2.5 Research Gap and Our Contribution

The literature contains two main types of deep anomaly detectors: in one group, there are efficient, lightweight and inherently explainable anomaly detection models, but are typically limited to detecting only one type of anomaly (and multiple models are required to detect different types of anomaly). In the other group we have powerful VLMs which can perform multi-type anomaly detection and segmentation but are computationally expensive. This identifies a clear research gap: the need for a unified, lightweight and efficient model with inherent explainability capable of multi-type anomaly detection and segmentation.

We introduce a lightweight extension of the FCDD [28] framework called MultiTypeFCDD that generates multi-channel anomaly heatmaps, with each channel representing a specific defect category. This design allows for the simultaneous detection and localization of multiple predefined anomaly types.

## 3 Proposed Method

### 3.1 Model

Our method builds upon the fully convolutional architecture in FCDD [24] which produces explainable anomaly heatmaps. The key novelty lies in the output layer. Unlike the original FCDD architecture which generates a single anomaly heatmap, we extend the architecture such that the output layer produces multi-channel anomaly heatmaps. Specifically, we replace the final layer with a  $1 \times 1$  convolutional layer with depth equal to the number of types of anomaly, enabling the model to produce a separate heatmap for each anomaly class. Figure 1 shows the outline of our proposed framework.

Let  $X_i \in \mathbb{R}^{h \times w \times c}, i \in \{1, \dots, N\}$  be the set of input images. Let  $M$  be the number of anomaly classes and  $y_{ik} \in \{0, 1\}$  be the binary labels for each anomaly class  $k \in \{1, \dots, M\}$  assigned to the image  $X_i$ . This indicates the presence (1) or absence (0) of the anomaly class. An image  $X_i$  is defined as Normal if all anomaly classes are absent, i.e.,  $\forall k, y_{ik} = 0$ . Let  $\phi(X_i; W) : \mathbb{R}^{h \times w \times c} \rightarrow \mathbb{R}^{u \times v \times M}$  be the fully convolutional network with weights  $W$ . A pseudo-Huber loss function is applied to the output of  $\phi$  and generates a low-resolution anomaly heatmap  $A_k(X_i) \in \mathbb{R}^{u \times v}$  for each class  $k$  defined as

$$A_k(X_i) = \sqrt{\phi(X_i; W)^2 + 1} - 1. \quad (1)$$

The overall anomaly score  $z_{ik}$  for any input image is computed as the L1-norm of the corresponding anomaly heatmap  $A_k(X_i)$ , defined as

$$z_{ik} = \frac{1}{u \cdot v} \|A_k(X_i)\|_1, \quad (2)$$

where  $u$  and  $v$  correspond to the dimensions of  $A_k$  which is the same for each heatmap. The heatmaps generated by the model are of lower resolution than

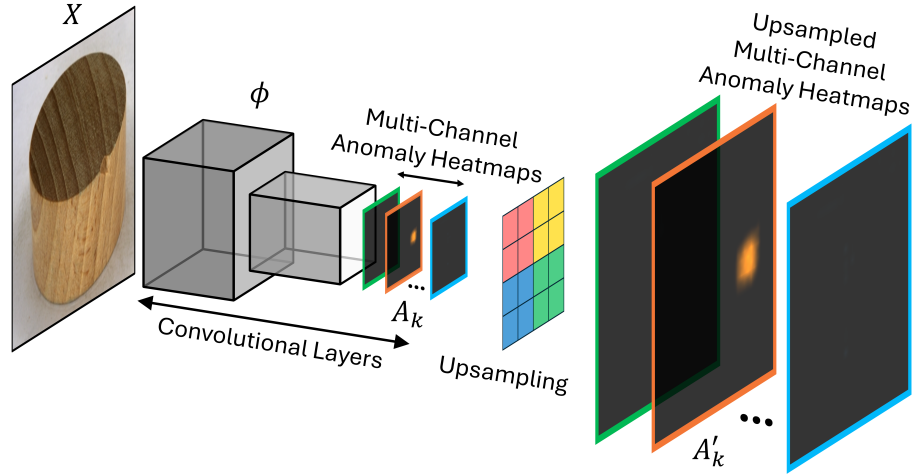


**Fig. 1.** Illustration of MultiTypeFCDD framework. An input image  $X$  is fed into a convolutional network  $\phi$  which produces multi-channel outputs  $A_k$  corresponding to different anomaly types. These outputs are then resized to heatmaps  $A'_k$  that match the input image dimensions.

the input due to downsampling through convolution and pooling layers. Therefore, we upsample each heatmap using bilinear interpolation to generate  $A'_k$  that matches the input image dimensions, thereby producing a one-to-one correspondence to each pixel in the anomaly heatmap to the input image.

### 3.2 Loss Function

The standard FCDD loss function is designed for binary anomaly detection where each image is either normal or anomalous. In our multi-type anomaly detection setting, each image may contain multiple anomaly classes. Therefore, we modify the FCDD loss function to accommodate each type of anomaly. The proposed objective function is defined as

$$\min_W \frac{1}{MN} \sum_{i=1}^N \sum_{k=1}^M (1 - y_{ik}) z_{ik} - y_{ik} \log(1 - e^{-z_{ik}}). \quad (3)$$

Using only image-level labels, the model learns to identify the discriminative regions in the images containing the target class and those without it. The loss function encourages the model to localise anomalies by maximising pixel-level anomaly scores in spatial regions where anomalies are present while suppressing the scores elsewhere, thereby enabling the generation of class-specific anomaly heatmaps in a weakly supervised manner.

## 4 Experimental Setting

### 4.1 Dataset

Many existing anomaly detection datasets like MVTec-AD [4] and VisA [42] focus on object-specific defects, where the anomalies are closely tied to the specific object. This makes them unsuitable for the task of multi-type anomaly detection, where our approach is designed to detect and differentiate various types of defects found across various objects.

To address this limitation, we adopt the Real-IAD dataset [38], which provides image-level and pixel-level annotations for various defect types commonly observed across a wide variety of objects. The Real-IAD dataset comprises 151,050 images of 30 objects, consisting of 99,721 normal images and 51,329 anomalous images, spanning 8 defect categories. Table 1 summarises the various defect codes used in the dataset.

**Table 1.** Defect codes and their definitions in the Real-IAD dataset.

Code	Defect Type	Code	Defect Type
AK	Pit	PS	Damage
BX	Deformation	QS	Missing Parts
CH	Abrasion	YW	Foreign Objects
HS	Scratch	ZW	Contamination

We follow the same train/test split procedure as in the original paper and use three training sets with noise ratios  $\alpha \in \{0.1, 0.2, 0.4\}$ , indicating the fraction of anomalous images in the training data.

### 4.2 Balanced Dataset Sampling: Redefining Epochs

Anomaly detection tasks inherently suffer from data imbalance, as datasets contain fewer anomalous samples than normal images. Given that we require images of various types of anomalies rather than “any” anomaly, the data imbalance problem becomes even more severe. Training a model on an imbalanced dataset can lead to overfitting to patterns in normal images and reduced sensitivity to anomalies [13, 30]. To address this, we adopt a balanced sampling strategy during training, inspired by the sampling procedure for binary anomaly detection in [24] (Appendix E), where images from each anomaly class, including normal, are uniformly sampled per iteration.

While this improves performance and enhances the model’s ability to distinguish among various anomalies and normal images, it has an important computational implication: the number of iterations required to complete an epoch increases. Unlike a standard training epoch, which process each image exactly

once, balancing requires the reshuffling and resampling of classes with fewer images, necessitating the analytical computation of the total number of iterations per epoch.

The problem is analogous to the generalised coupon collector problem [34], where each ‘‘coupon’’ corresponds to an image from a given class. Let each class  $i \in \{1, 2, \dots, n\}$  have a target quota of  $m_i$  (number of images per class) and is randomly chosen with equal probability. The expected number of iterations  $E[T]$  required to see each class  $i$  at least  $m_i$  times is given by the formulation

$$E[T] = n \int_0^\infty \left[ 1 - \prod_{i=1}^n (1 - S_{m_i}(t)e^{-t}) \right] dt, \quad (4)$$

where

$$S_{m_i}(t) = \sum_{k=0}^{m_i-1} \frac{t^k}{k!}$$

corresponds to the first  $m_i$  terms of the series expansion of  $e^t$ .

For large quotas, direct computation of this integral is practically infeasible. Therefore in practice, one can use Monte Carlo simulation to estimate  $E[T]$  empirically as

$$E[T] \approx \mu_T = \frac{1}{N_{\text{trials}}} \sum_{j=1}^{N_{\text{trials}}} T_j, \quad (5)$$

where  $T_j$  is the number of iterations in trial  $j$  until all quotas are met, and  $N_{\text{trials}}$  is the total number of Monte Carlo trials. This gives the empirical mean iterations per epoch, denoted as  $\mu_T$ . During training, images are processed in mini-batches. Therefore, the mean mini-batch iterations per epoch, which we refer to as balanced epochs, can be computed as  $\mu_T^{\text{batch}}$ .

Table 2 shows Monte Carlo simulation results (10000 iterations) on the three different Real-IAD training datasets across 9 image classes (8 anomaly classes and 1 normal class) at a mini-batch size of 32. When interpreted under the standard epoch definition (where each image is sampled exactly once), a balanced epoch corresponds to several standard epochs, e.g. at  $\alpha = 0.1$ , one balanced epoch equals 8.41 standard epochs. Therefore, even when the model appears to converge in only a few balanced epochs, it has actually been exposed to the data multiple times, achieving better class coverage and more stable learning.

**Table 2.** Monte Carlo simulation results to estimate iterations per balanced epoch.

$\alpha$	Total Images	Image Classes	$\mu_T^{\text{batch}}$	Std. Iterations	Std. Epochs
0.1	57,840	9	15,206.14	1807.5	8.41
0.2	57,840	9	14,128.68	1807.5	7.82
0.4	57,840	9	11,960.70	1807.5	6.62

### 4.3 Training Setup

**Model Architecture:** The backbone of the network employs the first three stages of an Inception-ResNet-v2 encoder [36] pre-trained on ImageNet [9], with all layers frozen to retain generic feature representations. The encoder is appended with a convolutional head which contains three sequential blocks: (1) two convolutional blocks ( $3 \times 3$  convolution with 512 filters + batch normalisation + ReLU), (2) a  $1 \times 1$  convolution layer with the number of output channels equal to the number of anomaly types, and (3) a differentiable function layer applying pseudo-Huber loss for each anomaly channel as given in Eq. 1.

**Hyperparameter Tuning:** For robust training, data augmentations were applied randomly to 50% of the images in the training dataset. These included random rotations within  $\pm 15^\circ$ , random translations within  $\pm 20$  pixels along both X and Y directions, and random brightness and contrast adjustments. The network was trained using the Adam optimiser with a mini-batch size of 32 with an initial learning rate of 0.0001.

**Hardware Configuration** All experiments were conducted on a desktop PC equipped with an NVIDIA RTX 4070 GPU and an AMD Ryzen 5 5500 CPU.

### 4.4 Evaluation Metrics

We follow the Real-IAD [38] benchmark protocol, where model performance is evaluated at both the image and pixel levels. At the image level, we report metrics such as Image-level AUROC (I-AUROC), Average Precision (AP), and max F1-score (F1m) to assess performance across multiple defect types. At the pixel level, Pixel-level AUROC (P-AUROC) and Area Under the Per-Region Overlap (AUPRO) [4] were computed. AUPRO captures region-wise localisation quality and penalises false detections on background areas, providing a robust measure of segmentation precision.

### 4.5 Benchmark Algorithms

We also report metrics for MultiTypeFCDD under a multi-class anomaly detection setting, because the modified framework with a single-channel anomaly output functions as a standard FCDD model that can be compared with state-of-the-art anomaly detectors, which identify the presence of anomalies but do not distinguish their types. Accordingly, we compare performance against PaDiM [7], CFlow [15], PatchCore [29], SimpleNet [23], DeSTSeg [41], RD [8], and UniAD [40] and report I-AUROC and AUPRO metrics.

## 5 Results

### 5.1 Multi-Type Anomaly Detection

The results of multi-type anomaly detection using our method are presented in Tables 3 and 4. At the image-level, mean I-AUROC reports over 94% across varying  $\alpha$  values, followed by similar increasing trends for mean AP and F1m. This indicates the model’s capability to discriminate between normal and anomaly-specific images. At the pixel-level, the the model maintains robust localisation performance with mean P-AUROC above 92% and steady AUPRO improvements as  $\alpha$  increases. In general, the model has strong capability of detecting various types of anomalies. However, it should be noted that certain anomaly types, such as Foreign Objects (YW) has lower performance values because the dataset contains fewer samples for this class compared to others and lacks consistent patterns when compared to classes like Scratch (HS). Figure 2 gives a visualisation of anomaly localisation across the eight defect classes for vaious objects at  $\alpha = 0.2$ . We have also added a visual comparison of the anomaly heatmaps (see Fig.3) for various  $\alpha$  values for a test object to illustrate the anomaly localisation performance of our model.

**Table 3.** Image-Level Multi-Type Anomaly Detection Performance.

Anomaly Type	$\alpha = 0.1$			$\alpha = 0.2$			$\alpha = 0.4$		
	I-AUROC	AP	F1m	I-AUROC	AP	F1m	I-AUROC	AP	F1m
Pit	92.4	47.9	51.1	95.7	62.5	60.7	93.7	50.5	51.7
Deformation	99.4	79.7	72.4	99.7	90.7	84.6	99.6	88.5	81.7
Abrasion	97.4	71.4	69.7	98.7	74.0	69.0	99.0	77.7	74.1
Scratch	91.1	56.6	52.0	92.7	56.4	56.4	92.9	58.3	52.5
Damage	97.1	37.1	45.5	98.9	57.0	56.4	98.3	46.7	50.6
Missing Parts	89.9	56.9	53.9	91.0	63.5	59.2	90.7	53.0	51.9
Foreign Objects	98.2	21.0	37.3	99.0	37.7	46.3	99.2	57.3	52.9
Contamination	91.5	77.2	72.2	93.0	77.8	74.9	93.1	81.0	75.6
Mean	94.6	56.0	56.8	96.1	64.9	63.4	95.8	64.1	61.4

### 5.2 Multi-Class Anomaly Detection

We also evaluate MultiTypeFCDD in a multi-class anomaly detection setting using a single-channel anomaly output. This allows for fair benchmarking against state-of-the-art multi-class anomaly detection methods, as summarised in Table 5. While unsupervised methods show degradation in performance as the proportion of anomalous samples in the training dataset increases, weakly supervised approaches like ours, even with just image-level labels, benefit from additional anomalous samples and show improved performance. MultiTypeFCDD

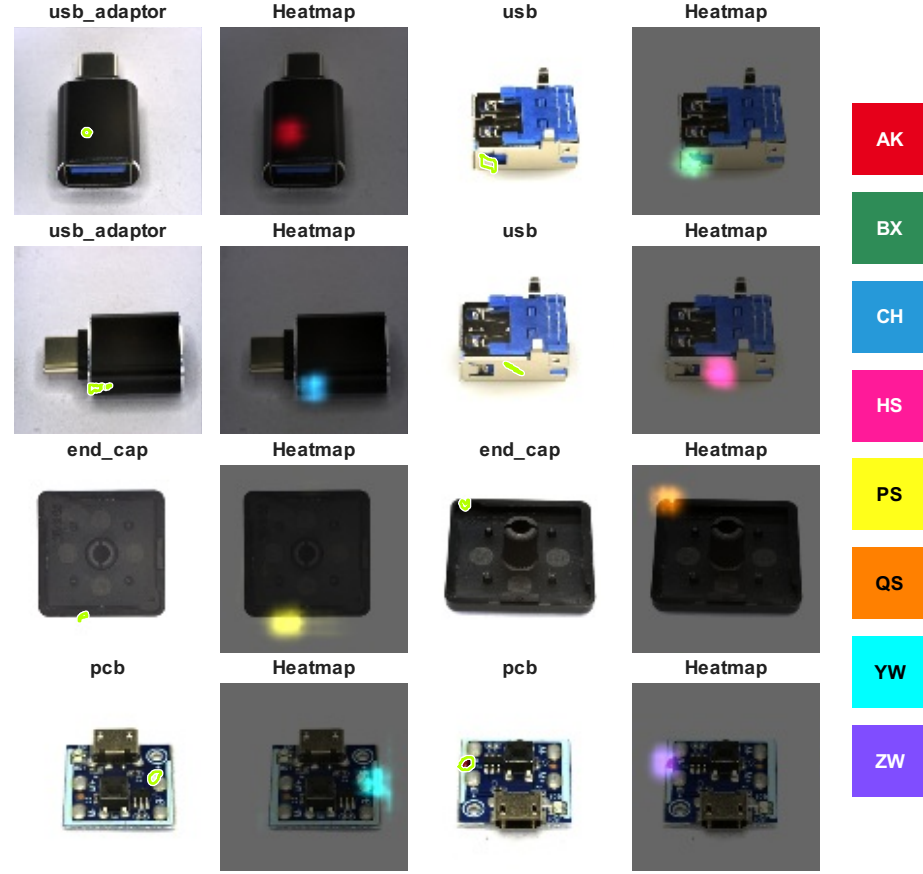


**Fig. 2.** Illustration of multi-type anomaly detection across different objects ( $\alpha = 0.2$ ). Each pair shows the object (left) with the ground-truth anomaly and its corresponding anomaly heatmap (right) for each anomaly category, with colours for each anomaly type indicated in the legend.

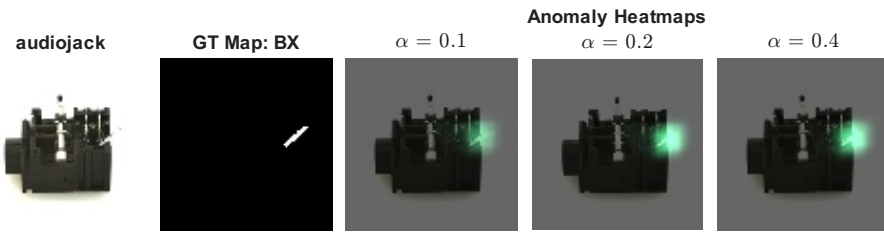


**Fig. 3.** Comparison of anomaly heatmaps for varying values of  $\alpha$ .

achieves consistently high AUROC scores across contamination levels, demon-

**Table 4.** Pixel-Level Multi-Type Anomaly Detection Performance.

Anomaly Type	$\alpha = 0.1$		$\alpha = 0.2$		$\alpha = 0.4$	
	P-AUROC	AUPRO	P-AUROC	AUPRO	P-AUROC	AUPRO
Pit	92.7	72.0	94.5	77.0	95.1	74.8
Deformation	97.7	81.3	97.0	82.9	97.2	80.2
Abrasion	97.6	75.0	97.0	66.2	97.7	76.5
Scratch	84.6	64.2	86.5	65.1	86.8	65.7
Damage	92.0	53.3	93.1	70.5	94.9	59.5
Missing Parts	85.4	69.1	82.0	66.8	87.8	74.8
Foreign Objects	96.6	39.9	94.6	40.6	95.5	38.7
Contamination	90.3	75.7	91.2	78.1	92.1	80.0
Mean	92.1	66.3	92.0	68.4	93.4	68.8

strating strong anomaly detection capability and generalisation across object categories. Although its AUPRO scores, which indicate anomaly localisation performance, are lower than those of methods such as PatchCore or SoftPatch, this is mainly because these approaches train separate models for each object class, allowing more precise localisation, and the results are averaged. In contrast, unified frameworks like MultiTypeFCDD and UniAD utilise a single model trained across all object classes, which makes fine-grained localisation more challenging but substantially reduces the total number of parameters, requiring only a fraction of the memory and computational overhead while maintaining competitive overall performance.

**Table 5.** Multi-Class Anomaly Detection Performance (I-AUROC / P-AUPRO). A \* indicates that the methods use a single unified model across all object classes.

Method	$\alpha = 0.1$		$\alpha = 0.2$		$\alpha = 0.4$		#Params (M)
	AUROC	AUPRO	AUROC	AUPRO	AUROC	AUPRO	
PaDiM [7]	81.9	86.4	80.1	86.5	77.0	86.1	68.9
CFlow [15]	83.9	90.7	79.6	90.7	78.0	90.2	30.4
PatchCore [29]	90.4	<b>94.2</b>	89.5	<b>93.9</b>	88.1	92.4	68.9
SoftPatch [20]	90.9	92.9	90.5	92.9	89.3	<b>92.5</b>	68.9
SimpleNet [23]	79.9	83.9	75.9	83.2	74.7	70.5	68.9
DeSTS [41]	85.6	86.9	80.3	83.2	74.4	75.5	37.9
RD [8]	<b>95.1</b>	87.6	94.9	83.2	94.7	81.5	68.9
UniAD* [40]	84.2	87.7	82.8	87.3	80.1	86.6	7.6
<b>MultiTypeFCDD*</b>	94.1	75.2	<b>95.5</b>	75.4	<b>96.4</b>	79.9	<b>5.5</b>

### 5.3 Computational Performance

To emphasise the practical deployability of our approach, we benchmark its computational footprint against MultiADS [32] presented in Table 6. MultiADS is a suitable baseline since it can segment multiple defect types similar to our method. However, it relies on image–text prompts to train a VLM, whereas our framework uses only image inputs and standard convolutional layers. Consequently, we do not perform a direct comparison under the multi-type anomaly detection setting.

It is to be noted that our model contains only 5.5 M parameters and occupies 19.7 MB of storage, over 80 times smaller than MultiADS, which requires 427.9 M parameters and 1.6 GB of memory. Furthermore, MultiTypeFCDD achieves significantly faster inference times, requiring only 69.9 ms per image on CPU and 1.7 ms on GPU, compared to 1824.3 ms (CPU) and 33.7 ms (GPU) for MultiADS. This comparison demonstrates that complex VLMs are not strictly necessary to achieve reliable multi-type anomaly detection. These findings align with our observations in Section 2.4, where large-scale VLMs are noted to be computationally and memory-intensive, restricting their usability in real-time or embedded systems [12, 25, 35]. In contrast, our lightweight architecture achieves competitive performance while substantially reducing memory and inference costs.

**Table 6.** Computational performance comparison.

Model	Parameters	Model Size	Inference Time (ms/img)	
	(M)	(MB)	CPU	GPU
MultiADS	427.9	1632.64	1824.3	33.7
<b>MultiTypeFCDD</b>	<b>5.5</b>	<b>19.7</b>	<b>69.9</b>	<b>1.7</b>

## 6 Conclusion

In this work, we proposed MultiTypeFCDD, a lightweight, unified, and explainable convolutional framework for multi-type anomaly detection. Our key contribution is a weakly supervised model that, using only image-level labels, can simultaneously detect anomalies across multiple object categories and, crucially, differentiate their specific types. This unified approach directly addresses two major gaps in existing literature. First, it eliminates the high overhead of training models per object category. Second, it differentiates between anomaly types, providing the diagnostic specificity that standard anomaly detectors lack. Furthermore, in contrast to massive VLMs that are computationally and memory-intensive, our model is designed as a lightweight and practical alternative, making it suitable for real-world, resource-constrained systems. We demonstrated

on the Real-IAD dataset that our framework retains competitive performance against complex state-of-the-art methods while significantly reducing parametric load and inference times. Future work could potentially include extending this framework to adaptively include open-set anomalies, enabling the model to identify and characterise previously unseen anomaly types without explicit retraining.

## References

1. Alzarooni, A., Iqbal, E., Khan, S.U., Javed, S., Moyo, B., Abdulrahman, Y.: Anomaly detection for industrial applications, its challenges, solutions, and future directions: A review. arXiv preprint arXiv:2501.11310 (2025)
2. Arrieta, A.B., Díaz-Rodríguez, N., Del Ser, J., Bennetot, A., Tabik, S., Barbado, A., García, S., Gil-López, S., Molina, D., Benjamins, R., et al.: Explainable artificial intelligence (xai): Concepts, taxonomies, opportunities and challenges toward responsible ai. *Information fusion* **58**, 82–115 (2020)
3. Bai, J., Wu, D., Shelley, T., Schubel, P., Twine, D., Russell, J., Zeng, X., Zhang, J.: A comprehensive survey on machine learning driven material defect detection. *ACM Computing Surveys* **57**(11), 1–36 (2025)
4. Bergmann, P., Batzner, K., Fauser, M., Sattlegger, D., Steger, C.: The mvtec anomaly detection dataset: a comprehensive real-world dataset for unsupervised anomaly detection. *International Journal of Computer Vision* **129**(4), 1038–1059 (2021)
5. Bogdoll, D., Nitsche, M., Zöllner, J.M.: Anomaly detection in autonomous driving: A survey. In: Proceedings of the IEEE/CVF conference on computer vision and pattern recognition. pp. 4488–4499 (2022)
6. Chen, Z., Chen, H., Imani, M., Imani, F.: Can multimodal large language models be guided to improve industrial anomaly detection? arXiv preprint arXiv:2501.15795 (2025)
7. Defard, T., Setkov, A., Loesch, A., Audigier, R.: Padim: a patch distribution modeling framework for anomaly detection and localization. In: International conference on pattern recognition. pp. 475–489. Springer (2021)
8. Deng, H., Li, X.: Anomaly detection via reverse distillation from one-class embedding. In: Proceedings of the IEEE/CVF conference on computer vision and pattern recognition. pp. 9737–9746 (2022)
9. Deng, J., Dong, W., Socher, R., Li, L.J., Li, K., Fei-Fei, L.: Imagenet: A large-scale hierarchical image database. In: 2009 IEEE conference on computer vision and pattern recognition. pp. 248–255. Ieee (2009)
10. Fernando, T., Gammulle, H., Denman, S., Sridharan, S., Fookes, C.: Deep learning for medical anomaly detection—a survey. *ACM Computing Surveys (CSUR)* **54**(7), 1–37 (2021)
11. Foorthuis, R.: On the nature and types of anomalies: a review of deviations in data. *International journal of data science and analytics* **12**(4), 297–331 (2021)
12. García-Martín, E., Rodrigues, C.F., Riley, G., Grahn, H.: Estimation of energy consumption in machine learning. *Journal of Parallel and Distributed Computing* **134**, 75–88 (2019)
13. Ghosh, K., Bellinger, C., Corizzo, R., Branco, P., Krawczyk, B., Japkowicz, N.: The class imbalance problem in deep learning. *Machine Learning* **113**(7), 4845–4901 (2024)

14. Gu, Z., Zhu, B., Zhu, G., Chen, Y., Tang, M., Wang, J.: Anomalygpt: Detecting industrial anomalies using large vision-language models. In: Proceedings of the AAAI conference on artificial intelligence. vol. 38, pp. 1932–1940 (2024)
15. Gudovskiy, D., Ishizaka, S., Kozuka, K.: Cflow-ad: Real-time unsupervised anomaly detection with localization via conditional normalizing flows. In: Proceedings of the IEEE/CVF winter conference on applications of computer vision. pp. 98–107 (2022)
16. He, H., Bai, Y., Zhang, J., He, Q., Chen, H., Gan, Z., Wang, C., Li, X., Tian, G., Xie, L.: Mambaad: Exploring state space models for multi-class unsupervised anomaly detection. *Advances in Neural Information Processing Systems* **37**, 71162–71187 (2024)
17. Jeong, J., Zou, Y., Kim, T., Zhang, D., Ravichandran, A., Dabeer, O.: Winclip: Zero/few-shot anomaly classification and segmentation. In: Proceedings of the IEEE/CVF Conference on Computer Vision and Pattern Recognition. pp. 19606–19616 (2023)
18. Jiang, M., Hou, C., Zheng, A., Hu, X., Han, S., Huang, H., He, X., Yu, P.S., Zhao, Y.: Weakly supervised anomaly detection: A survey. *arXiv preprint arXiv:2302.04549* (2023)
19. Jiang, X., Chen, Y., Nie, Q., Liu, J., Liu, Y., Wang, C., Zheng, F.: Toward multi-class anomaly detection: Exploring class-aware unified model against inter-class interference. *arXiv preprint arXiv:2403.14213* (2024)
20. Jiang, X., Liu, J., Wang, J., Nie, Q., Wu, K., Liu, Y., Wang, C., Zheng, F.: Softpatch: Unsupervised anomaly detection with noisy data. *Advances in Neural Information Processing Systems* **35**, 15433–15445 (2022)
21. Li, Z., Zhu, Y., Van Leeuwen, M.: A survey on explainable anomaly detection. *ACM Transactions on Knowledge Discovery from Data* **18**(1), 1–54 (2023)
22. Liu, F.T., Ting, K.M., Zhou, Z.H.: Isolation forest. In: 2008 eighth ieee international conference on data mining. pp. 413–422. IEEE (2008)
23. Liu, Z., Zhou, Y., Xu, Y., Wang, Z.: Simplenet: A simple network for image anomaly detection and localization. In: Proceedings of the IEEE/CVF conference on computer vision and pattern recognition. pp. 20402–20411 (2023)
24. Liznerski, P., Ruff, L., Vandermeulen, R.A., Franks, B.J., Kloft, M., Müller, K.R.: Explainable deep one-class classification. In: International Conference on Learning Representations (2021)
25. Marshall, J.A., Barron, A.B.: Are transformers truly foundational for robotics? *npj Robotics* **3**(1), 9 (2025)
26. Mokhtar, S., Mousakhan, A., Galessos, S., Tayyub, J., Brox, T.: Detect, classify, act: Categorizing industrial anomalies with multi-modal large language models. In: Proceedings of the Computer Vision and Pattern Recognition Conference. pp. 4058–4067 (2025)
27. Pang, G., Shen, C., Cao, L., Hengel, A.V.D.: Deep learning for anomaly detection: A review. *ACM computing surveys (CSUR)* **54**(2), 1–38 (2021)
28. Papa, L., Russo, P., Amerini, I., Zhou, L.: A survey on efficient vision transformers: algorithms, techniques, and performance benchmarking. *IEEE transactions on pattern analysis and machine intelligence* **46**(12), 7682–7700 (2024)
29. Roth, K., Pemula, L., Zepeda, J., Schölkopf, B., Brox, T., Gehler, P.: Towards total recall in industrial anomaly detection. In: Proceedings of the IEEE/CVF conference on computer vision and pattern recognition. pp. 14318–14328 (2022)
30. Ruff, L., Kauffmann, J.R., Vandermeulen, R.A., Montavon, G., Samek, W., Kloft, M., Dietterich, T.G., Müller, K.R.: A unifying review of deep and

shallow anomaly detection. *Proceedings of the IEEE* **109**(5), 756–795 (2021). <https://doi.org/10.1109/JPROC.2021.3052449>

31. Ruff, L., Vandermeulen, R., Goernitz, N., Deecke, L., Siddiqui, S.A., Binder, A., Müller, E., Kloft, M.: Deep one-class classification. In: International conference on machine learning. pp. 4393–4402. PMLR (2018)
32. Sadikaj, Y., Zhou, H., Halilaj, L., Schmid, S., Staab, S., Plant, C.: Multiads: Defect-aware supervision for multi-type anomaly detection and segmentation in zero-shot learning. *arXiv preprint arXiv:2504.06740* (2025)
33. Schölkopf, B., Platt, J.C., Shawe-Taylor, J., Smola, A.J., Williamson, R.C.: Estimating the support of a high-dimensional distribution. *Neural computation* **13**(7), 1443–1471 (2001)
34. Shank, N.B., Yang, H.: Coupon collector problem for non-uniform coupons and random quotas. *the electronic journal of combinatorics* pp. P33–P33 (2013)
35. Strubell, E., Ganesh, A., McCallum, A.: Energy and policy considerations for modern deep learning research. In: *Proceedings of the AAAI conference on artificial intelligence*. vol. 34, pp. 13693–13696 (2020)
36. Szegedy, C., Ioffe, S., Vanhoucke, V., Alemi, A.: Inception-v4, inception-resnet and the impact of residual connections on learning. In: *Proceedings of the AAAI conference on artificial intelligence*. vol. 31 (2017)
37. Tax, D.M., Duin, R.P.: Support vector data description. *Machine learning* **54**(1), 45–66 (2004)
38. Wang, C., Zhu, W., Gao, B.B., Gan, Z., Zhang, J., Gu, Z., Qian, S., Chen, M., Ma, L.: Real-iad: A real-world multi-view dataset for benchmarking versatile industrial anomaly detection. In: *Proceedings of the IEEE/CVF Conference on Computer Vision and Pattern Recognition*. pp. 22883–22892 (2024)
39. Yang, J., Mehta, N., Demirci, G., Hu, X., Ramakrishnan, M.S., Naguib, M., Chen, C., Tsai, C.L.: Anomaly-guided weakly supervised lesion segmentation on retinal oct images. *Medical image analysis* **94**, 103139 (2024)
40. You, Z., Cui, L., Shen, Y., Yang, K., Lu, X., Zheng, Y., Le, X.: A unified model for multi-class anomaly detection. *Advances in Neural Information Processing Systems* **35**, 4571–4584 (2022)
41. Zhang, X., Li, S., Li, X., Huang, P., Shan, J., Chen, T.: Destseg: Segmentation guided denoising student-teacher for anomaly detection. In: *Proceedings of the IEEE/CVF conference on computer vision and pattern recognition*. pp. 3914–3923 (2023)
42. Zou, Y., Jeong, J., Pemula, L., Zhang, D., Dabeer, O.: Spot-the-difference self-supervised pre-training for anomaly detection and segmentation. In: *European conference on computer vision*. pp. 392–408. Springer (2022)